Disruption of dual zygotic spindle assembly shows epigenetic asymmetry to be chromosome intrinsic

Long title: Dual zygotic spindle formation explains parental genome separation and its disruption shows that epigenetic asymmetry and differential reprogramming is chromosome intrinsic

Judith Reichmann[1], Bianca Nijmeijer[1], M. Julius Hossain[1], Manuel Eguren[1], Isabell Schneider[1], Antonio Z. Politi[1], M. Julia Roberti[1], Lars Hufnagel[1], Takashi Hiiragi[2] and Jan Ellenberg[1*]

[1]Cell Biology and Biophysics Unit, European Molecular Biology Laboratory, 69117 Heidelberg, Germany.

[2]Developmental Biology Unit, European Molecular Biology Laboratory, 69117 Heidelberg, Germany.

*corresponding author

In the early mammalian embryo, chromosomes are compartmentalised in a parent-of-origin specific manner, a feature thought to be important for their differential reprogramming Probst and Almouzni [1,2-4]. In mammals, pronuclei do not fuse after fertilisation but parental genomes are first replicated separately and then brought together after pronuclear envelope breakdown on the metaphase plate of the first mitosis [5,6]. Strikingly, maternal and paternal chromatin occupies distinct hemispheres in the nuclei of the two-cell embryo, and this separation only gradually decreases during subsequent stages of development [4,7]. Both the mechanism underlying parental genome separation and its functional importance for differential reprogramming are currently unclear. Here we reveal that the formation of two separate bipolar spindles around each parental pronucleus keeps maternal and paternal genomes apart during the first cleavage of the zygote. This mechanistic understanding allows us to test the requirement of genome separation for maintaining epigenetic asymmetry and its differential reprogramming by experimentally mixing the parental chromosomes. We show that establishment, maintenance and reprogramming of epigenetic asymmetry between the parental genomes is a chromosome intrinsic property and occurs independently of their compartmentalisation.

Despite its potential importance, how parental genome separation is achieved in mammals, for how long it is maintained, and if it is functionally required for differential epigenetic reprogramming is currently not understood. To generate the first quantitative description of parental genome separation in the early embryo, we measured the distribution of differentially labelled maternal and paternal centromeres by imaging the metaphase plate of live mouse embryos from the zygote to the 8-cell stage by light sheet microscopy[8]. Zygotes showed strong separation of the parental genomes with a degree of overlap of only 21% ± 13% (mean ± SD; n=31; p= 4.7E-24 by permutation, *t-test*),

which increased in the subsequent developmental stages to 40% ± 16% (Supplementary Fig. 1A-D). We confirmed this result by mapping the distribution of paternal chromatin during interphase in fixed embryos by labelling the paternal genome with the thymidine analogue EdU (5-Ethynyl-2´-deoxyuridine) (Supplementary Fig. 1E-I).

Although parental genomes are found after fertilisation as physically distinct pronuclei, it is their distribution on the first mitotic spindle that will determine their distribution in the nuclei of the first two blastomeres. We hypothesised that the striking separation of paternal genomes in the 2-cell embryo might be due to a specific arrangement of the zygotic spindle. Immunofluorescence analysis of zygotic mitosis revealed that microtubule asters accumulate around each pronucleus, forming two separate bipolar spindles after nuclear envelope breakdown (Fig. 1A). Subsequently, the two spindles align and come into close apposition to form one compound barrel-shaped bipolar system. To understand how such a dual spindle is assembled, we next imaged live embryos with fluorescently labelled MTOCs and spindle microtubules (Supplementary Movie 1) with high spatio-temporal resolution using our recently developed inverted light-sheet microscope[8] (Fig. 1B). Remarkably, in 11 out of 13 analysed zygotes at least one dual pole did not fuse after the spindles had parallelised, suggesting that the two spindles align closely but do not completely merge into one functional unit even in anaphase (Fig. 1A,B arrowheads, Supplementary Movie 1). To characterise the mechanism of this unusual dual spindle assembly further, we analysed the congression of maternal and paternal centromeres in relation to growing spindle microtubules in live zygotes. This confirmed that independent spindles form around each paternal genome and allowed us to define three phases of zygotic spindle assembly (Fig. 2A). A transient first phase (~3 min; 10.3 ± 3.5 min to 13. 4 ±4 min after NEBD), characterised by the clustering of cytoplasmic microtubule asters around the two pronuclei; is followed by phase 2 (~16 min; 14.5± 4 min to 30.7 ± 6.5 min after NEBD), where individual bipolar spindles assemble around each parental genome; and subsequently by phase 3 (~83 min; 46.7±17 min to 129.2 ± 16.5 min after NEBD), when the two spindles align and combine into one barrel shaped structure. To test if the two spindles are functionally independent, we measured the temporal correlation and direction of maternal and paternal chromosome congression (Supplementary Fig. 2A, B and Fig. 2A, B; for details see methods). Maternal and paternal chromosomes congressed already during phase 2, while the spindles were still separated (Supplementary Fig. 2A, B) and their congression was not correlated until shortly before anaphase, suggesting that they are moved by different microtubule systems (Supplementary Fig. 2C). Furthermore, the parental genomes were moved along different directions, as evidenced by the large difference between the angles of the two forming metaphase plates, which became parallel only during dual spindle alignment in phase 3 (Fig. 2B-D; Supplementary Fig. 2D, E). Consistent with this, tracking of growing microtubule tips showed two different directions of microtubule flow during

phase 2 (Supplementary Fig. 3A, B, Supplementary Movies 2, 3). This data shows that each of the two spindles around the parental genomes are functional for chromosome congression and act initially uncoupled from each other. Furthermore, when we increased the distance between two pronuclei and zygotic spindles by transient treatment with Nocodazole (Supplementary Fig. 3, Supplementary Movies 4-6), embryos initiated anaphase with two separate spindles, showing that the two spindles formed in the zygote are functional not just for chromosome congression but also segregation. Together these data strongly suggest that dual spindle formation and congression and biorientation of maternal and paternal chromosomes in two functionally independent microtubule systems provide the mechanism for parental genome separation.

This mechanism would predict that if only a single spindle is formed around both genomes, maternal and paternal chromosomes should be mixed. To test this prediction, we transiently treated zygotes with Monastrol, collecting both genomes in a single aster, and then allowed one bipolar spindle to reform after transiently depolymerising microtubules with Nocodazole (Supplementary Fig. 4, from here on referred to as MoNoc treated zygotes). MoNoc treated embryos captured and congressed chromosomes with a single spindle and showed a high degree of parental genome mixing approaching a completely random arrangement (Fig. 3). This is significantly different from untreated ($p = 9.9E-08$) or control zygotes ($p=0.0008$) in which the order of drug treatments is reversed (NocMo treated zygotes), which maintains dual spindle formation (Fig. 3; Supplementary Fig. 4). These data show that dual spindle formation is required for parental genome separation.

The spatial separation of maternal and paternal chromatin in distinct nuclear compartments of 2-cell embryos has been suggested to play a role in the differential epigenetic reprogramming of the parental genomes that is characteristic of early mammalian development [1-4]. At fertilisation, histone modifications as well as binding of Polycomb group (PcG) proteins and DNA methylation are highly asymmetric between oocyte and sperm chromatin due to their dramatically disparate differentiation programs. This asymmetry is subsequently removed in a parent specific manner and leads to epigenetically largely equalized genomes at the 8-cell or blastocyst stage, respectively [9-13]. Our new mechanistic understanding of how parental genomes are kept separate and the ability to experimentally mix them, now allowed us to test its importance for the resolution of epigenetic asymmetry, by assessing the degree and spatial distribution of several epigenetic modifications for which parental asymmetry has been reported, such as the DNA modifications 5-methylcytosine (5mC) and 5-hydroxymethylcytosine (5hmC), the histone modification H3K9me3 and the binding of the polycomb subunit protein Ring1B [10,13,14].

As expected, metaphase chromosomes in untreated zygotes showed strong epigenetic asymmetry in the two separate genome compartments. Also as expected, the asymmetry between individual chromosomes remained intact in embryos during the division from the 2 to the 4-cell stage, and the coverage of chromosomes by the epigenetic marks and their spatial compartmentalisation was highly reduced for 5mC, 5hmC and Ring1B, and increased for H3K9me3 by the 8-Cell stage, validating that our assay can detect the resolution of epigenetic asymmetry in early embryos (Fig. 4 and Supplementary Fig. 5). If genome separation was required for resolution of epigenetic asymmetry, we would expect that experimental mixing of maternal and paternal chromosomes in the zygote (Fig. 3) should affect epigenetic asymmetry between individual chromosomes in the 2-cell embryo and its subsequent resolution. Surprisingly, the epigenetic asymmetry in embryos with mixed parental genomes was indistinguishable from untreated and control embryos, consistent for all epigenetic modifications analysed (Fig. 4 and Supplementary Fig. 5A, B). The total amount of epigenetic modification (as judged by volume occupied by 5mC and 5hmC and the chromatin markers Ring1B and H3K9me3) remained unchanged in the division from 2 to 4-cell stage and showed the expected reduction for 5mC, 5hmC and Ring1B, and increase for H3K9me3, by the 8-cell stage (Supplementary Figs. 5 and 6). Taken together, these data show that parental epigenetic asymmetry is a chromosome-intrinsic property and that its reprogramming occurs independent of nuclear compartmentalisation.

We show here that zygotic dual spindle assembly provides the mechanism of parental genome separation in mammals (Figs 2 and 3). This extends our earlier study [15] that did not capture the dual spindle formation in zygotes due to insufficient spatio-temporal resolution, underlining the advantages of high speed light-sheet microscopy compared to confocal laser scanning. Our finding that establishment, maintenance and reprogramming of epigenetic asymmetry between the parental genomes is not dependent on their separate nuclear compartmentalisation suggests that these processes operate in a chromosome intrinsic mechanism independent of the nuclear distribution of the parental genomes (Fig. 4 and supplementary Figs 5 and 6). The striking phenomenon of dual spindle assembly around two spatially separated genomes in mouse, suggests that two spindles might also be found in zygotes from other species that maintain two pronuclei during DNA replication, and combine parental genomes only when entering M-phase. Indeed, consistent observations have been made in arthropods [5,6]. This model is also in agreement with the topological separation of parental chromosomes in human zygotes [16] and with reports of aberrant zygotic divisions into three or four blastomeres or bi-nucleated blastomeres in cattle and human [17-21]. These severe and relatively frequent zygotic division errors in mammals find their likely mechanistic explanation in a failure of the close alignment of the two zygotic spindles prior to anaphase.

Acknowledgments

We thank Nathalie Daigle for cloning of the EB3-mCherry plasmid. We thank Pierre Neveu and Melina Schuh kindly providing tdiRFP670 and tdEos-Cep192, respectively. We thank Niels Galjart for kindly providing full length Homo sapiens EB3 cDNA (NM_001303050.1). We thank EMBL's laboratory of animal resources for excellent support with mouse strains. We thank Petr Strnad for development and assistance of the inverted light sheet microscope. The EMBL Advanced Light Microscopy Facility is acknowledged for support in image acquisition and analysis. We thank Arivis for support in image analysis. We thank James Reddington and Stephanie Alexander for critical reading of the manuscript. This work was supported by funds from the European Research Council (ERC Advanced Grant "Corema", grant agreement 694236) to J.E. and by the European Molecular Biology laboratory (all authors). J.R. was further supported by the EMBL Interdisciplinary Postdoc Programme (EIPOD) under Marie Curie Actions COFUND; M.E. by the EMBO long-term postdoctoral fellowship and EC Marie Slodowska-Curie postdoctoral fellowship; M.J.R. by a Humboldt Foundation postdoctoral fellowship.

Author Contributions

J.E. and J.R. conceived the project and designed the experiments. J.R., B.N., M.E. and I.S. performed the experiments. M.J.R. supported the mouse EDU experiments. J.R., J.H. and A.P. analysed the data. T.H. and L.H. contributed to conception and design of the work. J.E. and J.R. wrote the manuscript. All authors contributed to the interpretation of the data and read and approved the final manuscript.

Competing financial interest

L.H. and J.E. are scientific co-founders and advisors of Luxendo GmbH (part of Bruker), that makes light sheet–based microscopes commercially available.

Material and Methods

Mouse strains and embryo culture.

Mouse embryos were collected from superovulated 8- to 24-week-old female mice according to the guidelines of EMBL Laboratory Animal Resources and cultured in 30-µl drops of G1 (Vitrolife) covered by mineral oil (Ovoil, Vitrolife). Embryos used for immunofluorescence were isolated from C57BL/6J x C3H/He F1 females, or EGFP-Tuba C57BL/6J x C3H/He F1 females, mated with C57BL/6J x C3H/He F1 males and fixed at different stages of zygotic mitosis. Embryos used for imaging of parental chromosomes were isolated from C57BL/6J x C3H/He F1 or H2BmCherry C57BL/6J x C3H/He F1 females mated with Mus Spretus males (*Mus musculus* (MMU) and *Mus spretus* (MSP) hybrid

embryo). Culture during imaging was performed as described [8] with minor modifications. In brief embryos were imaged in G1 medium covered with mineral oil with 5% CO_2 and 5% O_2 atmosphere. To achieve mixing of chromosomes embryos were cultured with 0.1 mM Monastrol for 5 hours followed by 0.01mM Nocodazole for 1 hour. Subsequently embryos were imaged or allowed to develop until the two cell stage and then synchronised with 0.01mM Nocodazole or 0.1mM Monastrol and then fixed. For controls the order of drug treatment was reversed in addition to a no drug treatment control.

Expression Constructs and mRNA Synthesis

Constructs used for mRNA synthesis were previously described: TALE-mClover (pTALYM3B15 Addgene plasmid 47878) [22], EB3-mEGFP [23], tdEos-Cep192 [24] (a kind gift from Melina Schuh). To generate EB3-mCherry full length Homo sapiens EB3 cDNA (NM_001303050.1, a generous gift from Niels Galjart) was tagged at the C-terminus with a tandem mCherry and cloned into the vector pGEMHE for mRNA production. To generate TALE-tdiRFP670, mRuby from pTALYM4SpiMi-01 [25](Addgene plasmid 47879) was replaced with tdiRFP670 (Addgene plasmid 45466, the tandem construct was a kind gift from Pierre Neveu). After linearization of the template with PacI, capped mRNA was synthesized using T7 polymerase (mMessage mMachine Ultra Kit, following manufacturer's instructions, Ambion) and dissolved in 11 µl water. mRNA concentrations were determined using a NanoDrop (Thermo Fisher Scientific).

Immunofluorescence

For imaging of the mitotic spindle embryos were fixed and extracted as described [26]. Embryos were blocked in 5% normal goat serum, 3% BSA in PBST (0.1% Trition X-100) and then incubated overnight in blocking solution at 4 °C at the following antibody dilutions:1:500 mouse anti-tubulin (Sigma T6199) to visualise microtubules, 1:500 rabbit anti-pericentrin (Abcam ab4448) for staining of MTOCs, 1:100 human anti-Crest (Europe Bioproducts CS1058) to stain centromeres. Embryos were washed 3x 5 minutes with 0.3% BSA in PBST then incubated with anti-mouse Alexa 488, anti-rabbit Alexa 546, anti-human Alexa 647 all 1:500 in 5% normal goat serum, 3% BSA in PBST (all (Thermo Fisher Scientific A11029, A11035, A21445 respectively) and 5ug/ml Hoechst33342 (Sigma) for 1 hour at room temperature. Embryos were washed with 0.3% BSA in PBST for 3x 5 minutes before imaging. For imaging of 5mC and 5hmC embryos were fixed for 20 minutes with 4% PFA in PBS. Embryos were washed 3 times in 1% BSA in PBS then extracted overnight in 1% BSA in PBS containing 0.5% Trition X-100 . Embryos were incubated for 1 hour at 37 °C in the presence of 10 µg/ml RNAse A (Sigma). Chromosomes were denatured by incubating the embryos in 4N HCL for 30 minutes at 37°C followed by neutralisation with 100mM Tris buffer (pH8) at room temperature. Embryos were blocked with 3% BSA and 5% normal goat serum in PBST and then incubated at 4C overnight with 1:3000 mouse

anti 5-methylcytosine (Diagenode C152000081) and 1:3000 rabbit anti 5-hydroxymethylcytosine (RevMab Biosciences 31-1111-00). Embryos were washed with 3% BSA in PBST for 3x 5 minutes then incubated with 1:1500 anti-rabbit Alexa 647 (Thermo Fisher Scientific A21245), 1:1500 anti-mouse Alexa 546 (Thermo Fisher Scientific A11030) and 100nM Yoyo-1 (Thermo Fisher Scientific Y3601) for 1 hour at room temperature. Embryos were then washed 3x for 5 minutes with 3% BSA in PBST and imaged.

Micromanipulation

Embryos were injected based on methods described previously [23] The injected volumes ranged between 10–15 pl (3%–5% of the embryo volume) of 0.125 – 0.3 µg/µl mRNA. mRNA-injected embryos were incubated at 37°C for 4–6 hr in G1 medium as described above to allow recombinant protein expression. For labelling of MTOCs and microtubule tips MMU zygotes were injected with mRNA encoding tdEos-Cep192 and EB3-mCherry. For differential labelling of maternal and paternal centromeres MMU x MSP embryos were injected with mRNA encoding fluorescent proteins fused to TALEs specific to the different centromeric satellite repeats as described previously [25].

Embryo Imaging

Time-lapse image acquisitions were performed using a previously described in-house-built inverted light-sheet microscope [8]. For imaging MTOCs and microtubules stacks of 101 images with 520nm between planes were acquired simultaneously for mCherry and EGFP signals at 45 sec time intervals. Fixed embryos stained for spindle components and epigenetic marks were imaged on a SP8 Leica confocal microscope equipped with a 63× C-Apochromat 1.2 NA water immersion objective lens. Images of embryos stained for spindle components or epigenetic marks were acquired at 90nm XY and 360nm Z.

Image processing and analysis

Images of embryos stained and fixed for spindle markers were deconvolved using the Huygens remote manger (Scientific Volume Imaging) and maximum intensity projected in Arivis (arivis Vision4D). Time-lapse images were processed for extraction of raw camera data as described [8]. Time-lapse movies were generated as described [8] or exported from Arivis. Phases of zygotic mitosis were scored manually according to spindle morphology and presence of two bi-polar or single barrel shaped spindle. Spindles were segmented using an Arivis inbuilt intensity threshold filter. Chromosomes were segmented using an in house developed MATLAB segmentation pipeline based on intensity threshold and connected component analysis. Shape and direction of chromosomes are represented using Eigen value and Eigen vector of the segmented chromosomes in order to measure

chromosome congression and the angle between parental chromosomes. Segmentation of 5mC and 5hmC signals was performed using a script developed in MATLAB that quantifies the distribution of the signals and their correlation using bright pixels. Segmentation of maternal and paternal centromeres was performed using an in house developed MATLAB segmentation pipeline and the mixing between parental centromeres was measured using the overlap between their 3D convex hulls. More details in Supplemental Material and methods

References

1 Probst, A. V. & Almouzni, G. Pericentric heterochromatin: dynamic organization during early development in mammals. *Differentiation* **76**, 15-23, doi:10.1111/j.1432-0436.2007.00220.x (2008).

2 Duffie, R. & Bourc'his, D. Parental epigenetic asymmetry in mammals. *Curr Top Dev Biol* **104**, 293-328, doi:10.1016/B978-0-12-416027-9.00009-7 (2013).

3 De La Fuente, R., Baumann, C. & Viveiros, M. M. ATRX contributes to epigenetic asymmetry and silencing of major satellite transcripts in the maternal genome of the mouse embryo. *Development* **142**, 1806-1817, doi:10.1242/dev.118927 (2015).

4 Mayer, W., Smith, A., Fundele, R. & Haaf, T. Spatial separation of parental genomes in preimplantation mouse embryos. *J Cell Biol* **148**, 629-634 (2000).

5 Snook, R. R., Hosken, D. J. & Karr, T. L. The biology and evolution of polyspermy: insights from cellular and functional studies of sperm and centrosomal behavior in the fertilized egg. *Reproduction* **142**, 779-792, doi:10.1530/REP-11-0255 (2011).

6 Kawamura, N. Fertilization and the first cleavage mitosis in insects. *Dev Growth Differ* **43**, 343-349 (2001).

7 Mayer, W., Niveleau, A., Walter, J., Fundele, R. & Haaf, T. Demethylation of the zygotic paternal genome. *Nature* **403**, 501-502, doi:10.1038/35000654 (2000).

8 Strnad, P. *et al.* Inverted light-sheet microscope for imaging mouse pre-implantation development. *Nat Methods* **13**, 139-142, doi:10.1038/nmeth.3690 (2016).

9 Surani, M. A. Reprogramming of genome function through epigenetic inheritance. *Nature* **414**, 122-128, doi:10.1038/35102186 (2001).

10 Iurlaro, M., von Meyenn, F. & Reik, W. DNA methylation homeostasis in human and mouse development. *Curr Opin Genet Dev* **43**, 101-109, doi:10.1016/j.gde.2017.02.003 (2017).

11 Borsos, M. & Torres-Padilla, M. E. Building up the nucleus: nuclear organization in the establishment of totipotency and pluripotency during mammalian development. *Genes Dev* **30**, 611-621, doi:10.1101/gad.273805.115 (2016).

12 Cantone, I. & Fisher, A. G. Epigenetic programming and reprogramming during development. *Nat Struct Mol Biol* **20**, 282-289, doi:10.1038/nsmb.2489 (2013).

13 Puschendorf, M. *et al.* PRC1 and Suv39h specify parental asymmetry at constitutive heterochromatin in early mouse embryos. *Nat Genet* **40**, 411-420, doi:10.1038/ng.99 (2008).

14 Gill, M. E., Erkek, S. & Peters, A. H. Parental epigenetic control of embryogenesis: a balance between inheritance and reprogramming? *Curr Opin Cell Biol* **24**, 387-396, doi:10.1016/j.ceb.2012.03.002 (2012).

15 Courtois, A., Schuh, M., Ellenberg, J. & Hiiragi, T. The transition from meiotic to mitotic spindle assembly is gradual during early mammalian development. *J Cell Biol* **198**, 357-370, doi:10.1083/jcb.201202135 (2012).

16 van de Werken, C. *et al.* Paternal heterochromatin formation in human embryos is H3K9/HP1 directed and primed by sperm-derived histone modifications. *Nat Commun* **5**, 5868, doi:10.1038/ncomms6868 (2014).

17 Kligman, I., Benadiva, C., Alikani, M. & Munne, S. The presence of multinucleated blastomeres in human embryos is correlated with chromosomal abnormalities. *Hum Reprod* **11**, 1492-1498 (1996).
18 Hardy, K., Winston, R. M. & Handyside, A. H. Binucleate blastomeres in preimplantation human embryos in vitro: failure of cytokinesis during early cleavage. *J Reprod Fertil* **98**, 549-558 (1993).
19 Pickering, S. J., Taylor, A., Johnson, M. H. & Braude, P. R. An analysis of multinucleated blastomere formation in human embryos. *Hum Reprod* **10**, 1912-1922 (1995).
20 Destouni, A. *et al.* Zygotes segregate entire parental genomes in distinct blastomere lineages causing cleavage-stage chimerism and mixoploidy. *Genome Res* **26**, 567-578, doi:10.1101/gr.200527.115 (2016).
21 Egashira, A. *et al.* Developmental capacity and implantation potential of the embryos with multinucleated blastomeres. *J Reprod Dev* **61**, 595-600, doi:10.1262/jrd.2015-052 (2015).
22 Burton, A. & Torres-Padilla, M. E. Epigenetic reprogramming and development: a unique heterochromatin organization in the preimplantation mouse embryo. *Brief Funct Genomics* **9**, 444-454, doi:10.1093/bfgp/elq027 (2010).
23 Schuh, M. & Ellenberg, J. Self-organization of MTOCs replaces centrosome function during acentrosomal spindle assembly in live mouse oocytes. *Cell* **130**, 484-498, doi:10.1016/j.cell.2007.06.025 (2007).
24 Clift, D. & Schuh, M. A three-step MTOC fragmentation mechanism facilitates bipolar spindle assembly in mouse oocytes. *Nat Commun* **6**, 7217, doi:10.1038/ncomms8217 (2015).
25 Miyanari, Y., Ziegler-Birling, C. & Torres-Padilla, M. E. Live visualization of chromatin dynamics with fluorescent TALEs. *Nat Struct Mol Biol* **20**, 1321-1324, doi:10.1038/nsmb.2680 (2013).
26 Kitajima, T. S., Ohsugi, M. & Ellenberg, J. Complete kinetochore tracking reveals error-prone homologous chromosome biorientation in mammalian oocytes. *Cell* **146**, 568-581, doi:10.1016/j.cell.2011.07.031 (2011).

Figure legends

Figures

Figure 1. Microtubule balls formed around each pro-nucleus after NEBD mature into individual bi-polar spindles followed by their fusion into a barrel-shaped spindle. (A) Immunofluorescence staining of the mouse zygote fixed at consecutive stages of development. Shown are z-projected images of confocal sections of zygotes at prophase; early pro-metaphase, late pro-metaphase, early metaphase; late metaphase and anaphase. Microtubules (green), Pericentrin (magenta), Crest (grey), and DNA (blue) are shown. Scale bar, 5 µm. (B) Live cell time-lapse-imaging of zygotes expressing EB3-mCherry (green) and tdEos-Cep192 (magenta). Dashed ellipsoids trace spindle outline. Scale bar, 10 µm. White arrows indicate poles (A, B).

Figure 2. Spindle assembly and chromosome dynamics in the zygote are defined by three different phases. (A) Live cell time-lapse-imaging of zygotes expressing fluorescent TALEs to label maternal (magenta) and paternal (cyan) chromosomes and EB3-mCherry (white). Phase 1 (blue): Microtubule ball formation around pronuclei. Phase 2 (red): Bi-polarisation of maternal and paternal spindle. Phase 3 (green): Formation of single barrel shaped spindle. Lower row, segmentation of paternal (cyan) and maternal (magenta) spindles in Phase 1 and Phase 2 and single bipolar spindle in Phase 3 (grey). (B) Schematic of measurements. (C,D) Angle between maternal and paternal chromosome axis over time for a single embryo (C) and averaged for 12 embryos (D) are shown. Phase 1, blue; Phase 2, red; Phase 3, green.

Figure 3. Distribution of paternal and maternal centromeres in control, NocMo and MoNoc treated zygotes. (A) Differential labelling of maternal (magenta) and paternal (cyan) centromeres through distinction of SNPs by fluorescent TALEs. Mitotic spindle is labelled with EB3-mCherry (grey). Representative z-projected images of parental chromosome distribution in untreated, MoNoc and NocMo zygotes. Scale bar, 10 µm. (B) Degree of overlap between 3D convex hulls and parental chromosomes for untreated (n=31), MoNoc (n=16), NocMo (n=12) zygotes and embryos with *in silico* randomised distribution (n=40) (see Supplementary Fig. 1 and methods for details).

Figure 4. Epigenetic marks in mixed and unmixed embryos. (A) Immunofluorescence staining of zygotes, untreated, NocMo and MoNoc embryos at the 2-cell and 8-cell stage. Shown are z-projected images of confocal sections. Top panel shows 5mC and 5hmC staining (magenta, cyan) (salt and pepper distribution is expected based on results on parental chromosome distributions as determined in SF1 at the 2-cell stage). Middle panel shows DNA staining (white). Bottom panel shows chromosome surface (grey) and top 50% intensity pixels of 5mC (magenta) and 5hmC (cyan) printed as solid colours (see methods for details). Scale bar, 10 µm.

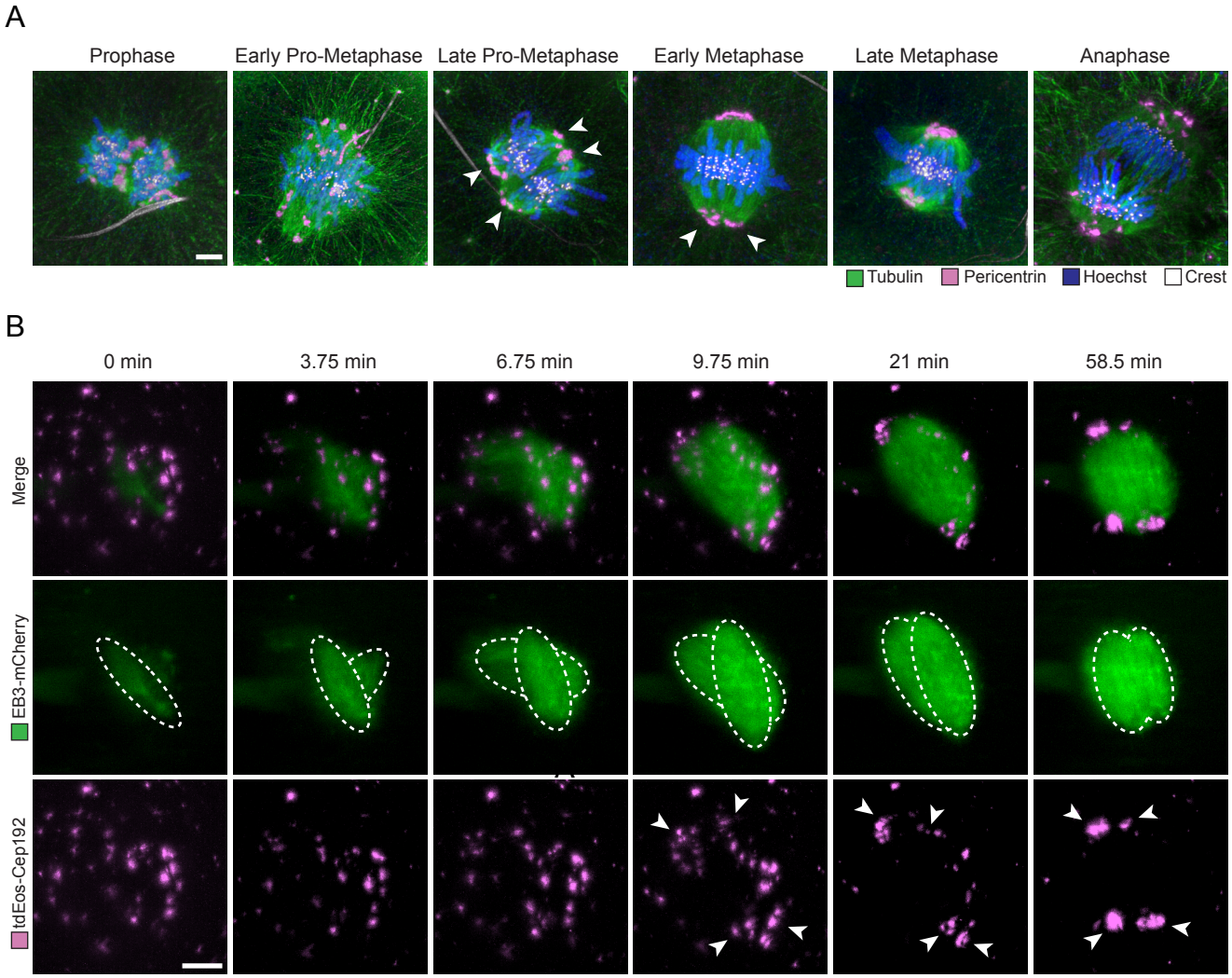

Figure 1

A

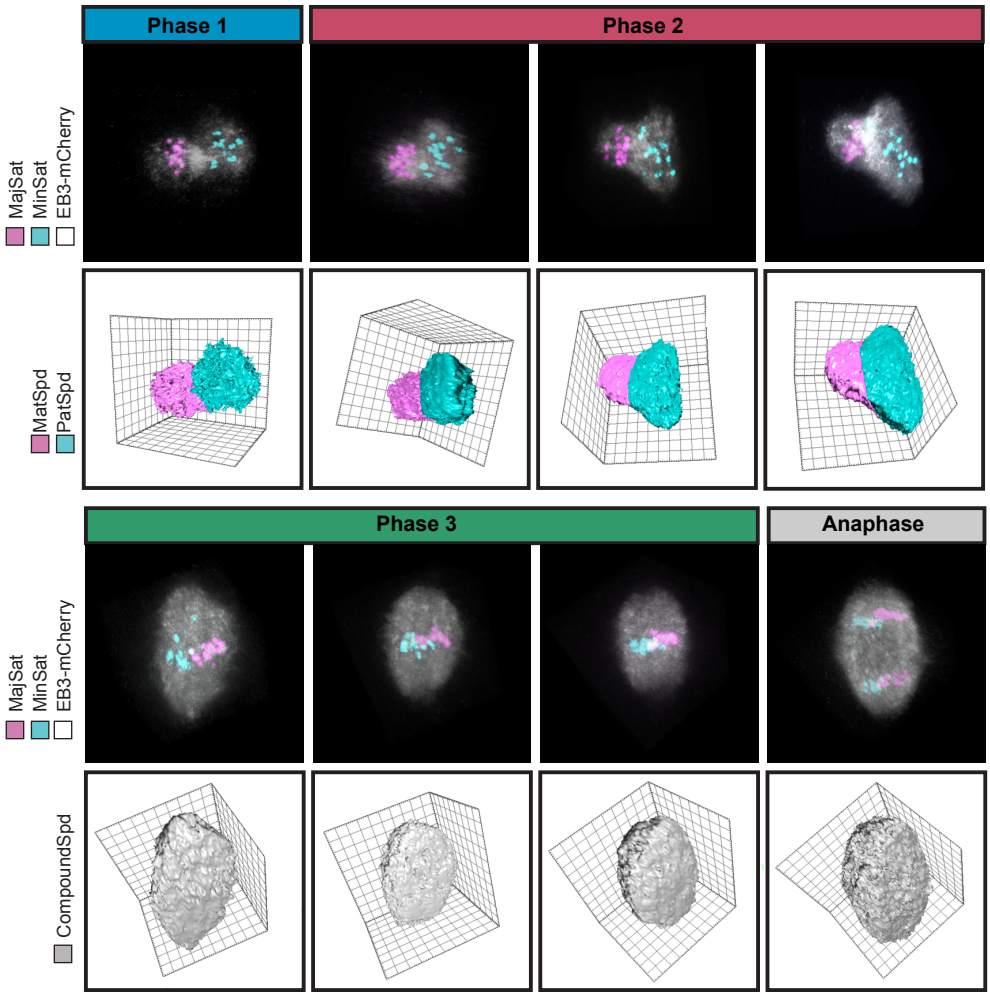

B

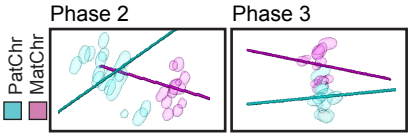

C

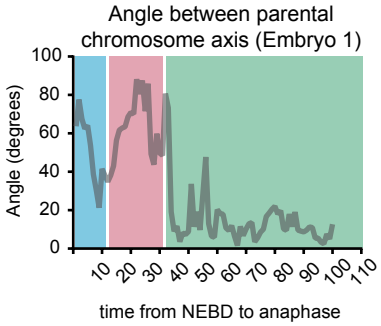

D

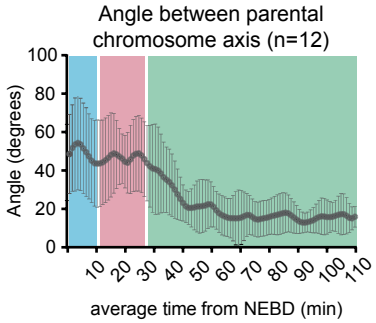

Figure 2

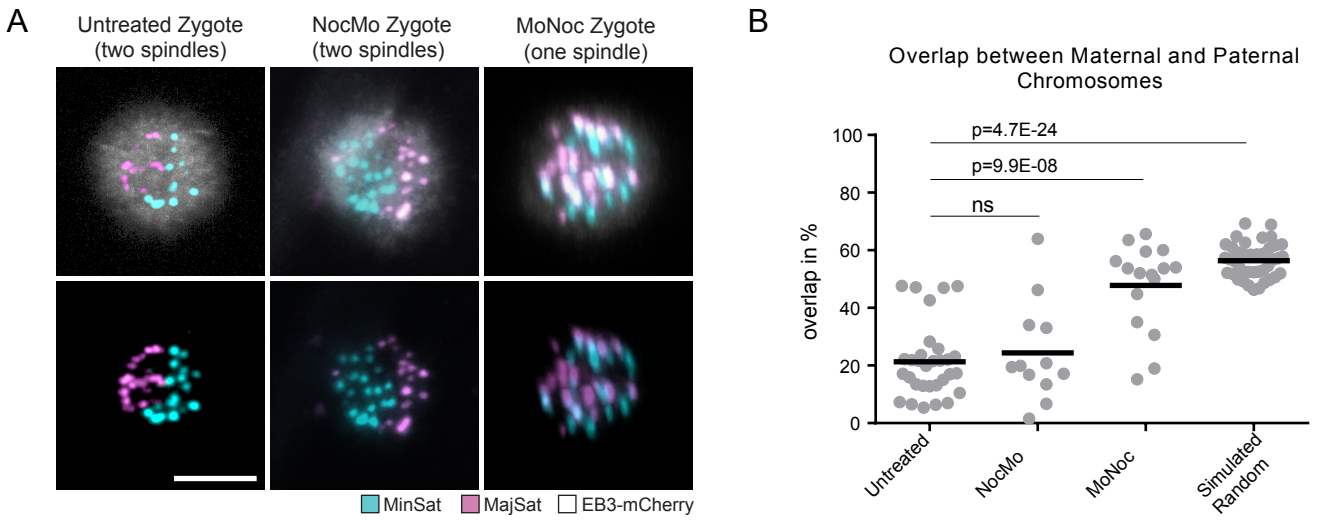

Figure 3

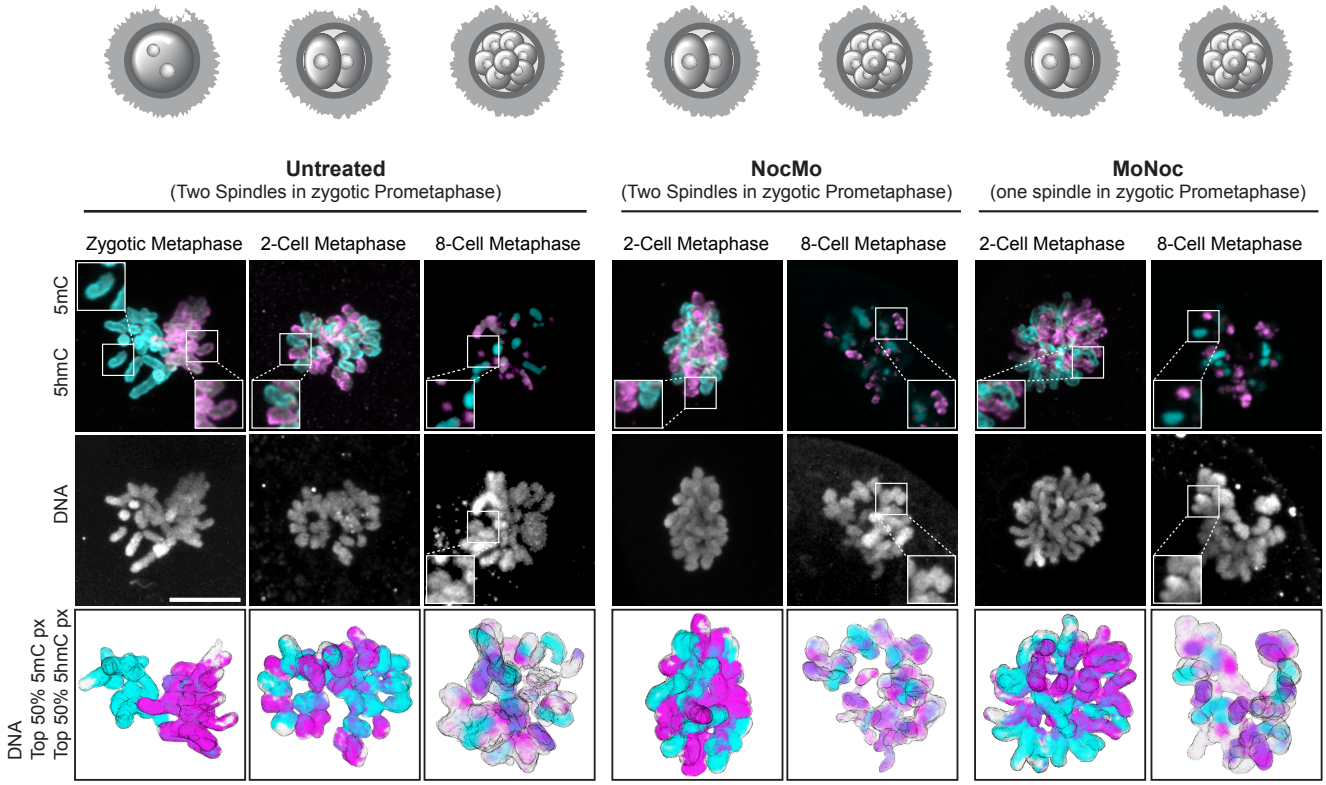

Figure 4